Graphene on weakly interacting metals: Dirac states versus surface states

Wouter Jolie,* Fabian Craes, and Carsten Busse
II. Physikalisches Institut, Universität zu Köln, Zülpicher Straße 77, 50937 Köln, Germany
(Received 1 November 2014; revised manuscript received 4 February 2015; published 13 March 2015)

We investigate the interplay between graphene and different, weakly interacting metal substrates by measuring the local density of states of the surface with scanning tunneling spectroscopy. Energy-resolved Friedel oscillations, confined states, and a prominent signal in point spectra are found after intercalating several monolayers of silver between graphene and Ir(111) and correspond to the shifted surface state of silver. These features outweigh spectroscopic signatures of graphene, which are retrieved when the amount of silver is reduced to one monolayer. Hence, suppressing the surface states of the metal substrate enhances the sensitivity to the Dirac states of quasi-free-standing graphene.

DOI: 10.1103/PhysRevB.91.115419 PACS number(s): 73.63.Hs, 73.22.Pr, 73.20.At, 73.20.−r

I. INTRODUCTION

Epitaxial growth on metal surfaces is a well-established procedure to prepare extended and defect-free sheets of graphene [1–3], but also novel two-dimensional materials (2DMs) can be grown by this method, as for example hexagonal boron nitride [4], the transition-metal dichalcogenides MoS_2 and WS_2 [5,6], or silicene [7]. Very often, the interaction between the metal substrate and the ultrathin layer on top of it is weak enough to allow for studies of the characteristic properties of 2DMs using surface science methods [8–10]. However, especially for extremely surface-sensitive methods such as scanning tunneling microscopy and spectroscopy (STM/STS), a disentanglement of the electronic properties of the substrate and the overlayer becomes rather difficult and in many cases impossible: For example, a clear signature of the Dirac point of graphene (gr) is absent in point spectra taken on, e.g., gr/Ag(111) [11] or gr/Cu(111) [3].

A special challenge arises when the Dirac states coexist with metal surface states with similar dispersion relations $E(k)$: In such a case, confined electronic states on nanometer-sized graphene flakes (graphene quantum dots, GQDs) on Ir(111) have been attributed to Dirac states of graphene [12,13], the surface state of Ir(111) [14], or a mixture of both [15]. A clear distinction is only possible in favorable cases as found for gr/Au(111) [16] or when the surface state is purposefully suppressed as for gr/O/Ir(111) [17].

Here, we present a detailed study of the mutual interplay between graphene and different metal substrates with respect to the resulting electronic structure. We study epitaxial graphene on a rather thick Ag(111) film on Ir(111) as a model system for gr/Ag(111), graphene on a monolayer of Ag(111)/Ir(111), and graphene on pristine Ir(111). All systems have in common that their interaction with the carbon sheet is weak enough to render the graphene quasi-free-standing, that is, free of strong localized bonds to the substrate. For the case of gr/Ir(111), this is evidenced by the observation of the Dirac cone in angle-resolved photoemission spectroscopy (ARPES) [9]. For the case of silver, ARPES measurements have shown that intercalating one monolayer (ML) of silver between graphene and Re(0001) almost completely recovers the linear Dirac cone which is absent without the intercalant due to the strong interaction of Re with graphene [18]. A similar observation is found when intercalating 1 ML between graphene and Ni(111) [19]. One property characteristic for a weakly interacting substrate under graphene, namely, intervalley scattering [20], has been reported for graphene on Ag(111) [11]. In addition, both Ag(111) and Ir(111) feature a surface state with a parabolic dispersion around the Γ point, which has a positive effective mass m^* for the case of Ag(111) and a negative m^* for Ir(111). As we will show in the following, for just one monolayer of Ag(111) on Ir(111), both surface states are suppressed, allowing a systematic investigation of the mutual interplay in our study.

STS enables a local determination of the electronic structure as it can determine the local density of states (LDOS) in dependence on the energy E. Even a full determination of the dispersion relation $E(k)$ ($k = k_\parallel$ is the in-plane crystal momentum) becomes possible when interference patterns of electronic states are analyzed. Such patterns can be either found in extended systems in the form of standing waves in the vicinity of one-dimensional defects or in the form of eigenmodes with discrete values of E and k when the states are confined to nanometer-sized quantum dots [21]. Both approaches will be used in our study.

The paper is structured as follows: After introducing the experimental setup and preparation techniques (Sec. II), in Sec. III we investigate the electronic properties of our model substrate [a thick film of Ag(111)/Ir(111)] with special emphasis on the surface state and the changes induced by the presence of graphene on top of this substrate. The additional effect arising when electronic states are confined by GQDs is introduced in Sec. IV. Finally, we study a system where conflicting surface states are partially suppressed, namely, graphene on top of one ML of Ag(111) on Ir(111) in Sec. V and conclude our work in Sec. VI.

II. EXPERIMENTAL SETUP AND SAMPLE PREPARATION

The sample is prepared in an ultrahigh vacuum (UHV) chamber at a base pressure lower than $p = 2 \times 10^{-10}$ mbar. The Ir(111) single crystal is cleaned by cycles of Ar^+ ion bombardment, then exposed to oxygen at 1125 K and annealed at 1475 K. For graphene growth, we apply two temperature programed growth (TPG) steps [22], adsorbing ethylene as

*wjolie@ph2.uni-koeln.de

a precursor at room temperature followed by annealing at 1475 K. We evaporate silver from a crucible with a rate of 0.575 Å/min (determined with a quartz crystal microbalance) with the sample at room temperature and obtained an Ag film with a nominal thickness of 15 ML. Heating the sample to $T = 750$ K enables diffusion of the GQDs to the surface as shown in Ref. [16] for the case of GQDs buried under a thin gold film. We find GQDs of various sizes on and embedded in silver. Low-energy electron diffraction shows that the silver film has a (111) orientation. In the following, we will refer to the uncovered silver film as 15 ML Ag(111)/Ir(111) and to the graphene covered areas as gr/15 ML Ag(111)/Ir(111).

After preparation, the sample is transferred (in UHV) to a second chamber where STM and STS measurements are performed at a base pressure of $p < 3 \times 10^{-11}$ mbar. We use a low-temperature scanning tunneling microscope operating at 5 K with a tungsten tip. We mainly prepare the tip by repeatedly dipping it into the surface with open feedback loop at a constant voltage of several volts to minimize the contribution of the LDOS of the tip. For STM, we apply a voltage V to the sample and detect a tunneling current I. For STS, we record a signal approximating the LDOS of the surface obtained by measuring the derivative dI/dV and normalizing it by I/V [23]. The energy of the detected states is given by $E = e \times V$, hence, $E_F = 0$ eV. We use a lock-in technique with a frequency in the range of 850–950 Hz and a modulation amplitude of $V_{mod} = 4$–10 mV, resulting in a lower limit of the experimental resolution [24] of $\Delta E \approx \sqrt{(3.3k_BT)^2 + (1.8eV_{mod})^2} \leqslant 0.02$ eV. All STM and STS measurements were acquired in constant current mode.

III. AG(111) SURFACE STATE

As the first step, we characterize the substrate used in this study, namely, 15 ML Ag(111)/Ir(111). An STM topography without any graphene is shown in Fig. 1(a) in yellow (gray) together with several dI/dV maps in blue (dark gray) recorded at different energies E (indicated in the images) on the same area. Standing wave patterns in the spectroscopic maps are evident, with a wavelength λ that depends on E [see Fig. 1(b)]. These features are typically interpreted as energy-resolved Friedel oscillations and indicate the presence of a surface state [25–27], as should be expected for Ag(111) [28]. On the upper terrace, the scattering at one single elongated edge is detected, resulting in a wave train normal to the edge. On the lower terrace, a second edge visible at the top of the STM image produces an additional wave train, thus causing an interference pattern due to the superposition of both standing waves evolving in different directions.

The underlying dispersion relation $E(k)$ of the surface state can be extracted from the measured values for λ using the relation [29] $k = \frac{\pi}{\lambda}$ in analogy to an interference pattern between ingoing and outgoing waves. The result for three different terraces is shown in Fig. 2. We fit the dispersion of the energy-resolved Friedel oscillations with a parabolic band (black line) to obtain the surface state energy at $k = 0$, E_0, and the effective mass m^* of the surface state. The resulting values for E_0 and m^*/m (with m defined as the free-electron mass) are given in the figure.

Our results can be compared to the behavior of the silver surface state on an Ag(111) single crystal [28] shown in olive in Fig. 2 with the corresponding values for E_0 and m^*/m. We find a good agreement of the effective masses. However, the bands clearly differ in their surface state energy: For the case of 15 ML Ag(111)/Ir(111), the surface state is shifted above the Fermi energy, from $E_0 = -0.075(5)$ to 0.011(5) eV.

In the next step, we compare dI/dV spectra (representing the LDOS) taken on 15 ML Ag(111)/Ir(111) and gr/15 ML Ag(111)/Ir(111) (see Fig. 3). The normalized spectrum measured on 15 ML Ag(111)/Ir(111) [black line in Fig. 3(b)]

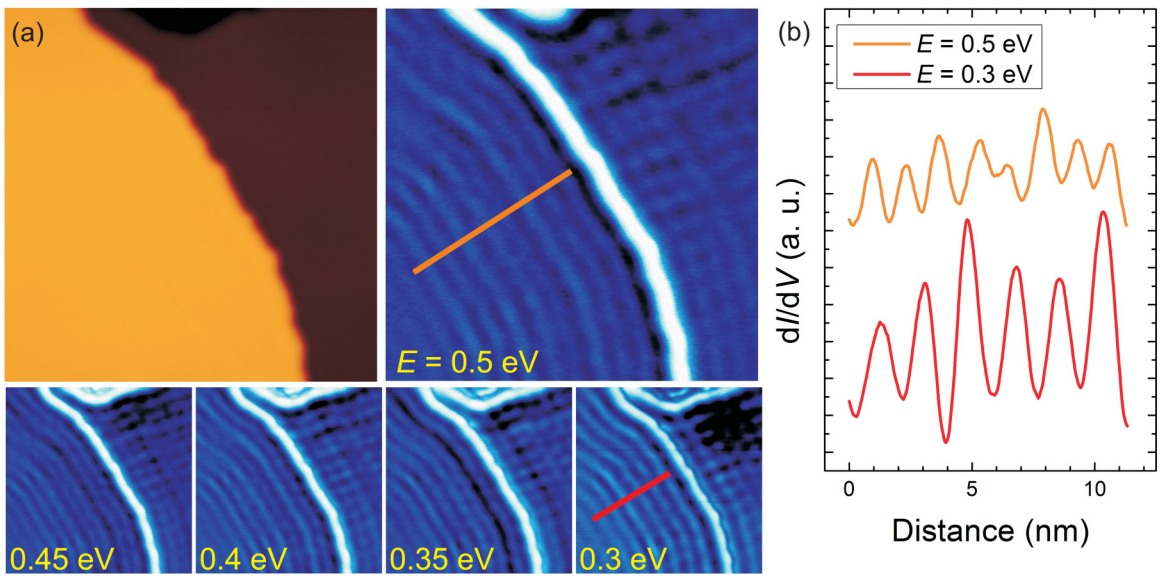

FIG. 1. (Color online) (a) STM image of 15 ML Ag(111)/Ir(111) ($I = 0.1$ nA, $U = 0.45$ V, image size 22×22 nm^2), together with several dI/dV maps recording the oscillating LDOS on the surface at the indicated energies E. (b) Line profiles of the observed energy-resolved Friedel oscillations recorded at $E = 0.5$ and 0.3 eV revealing a change in the wavelength with energy. They are obtained along the line drawn in the corresponding maps. The profiles are stacked for clarity.

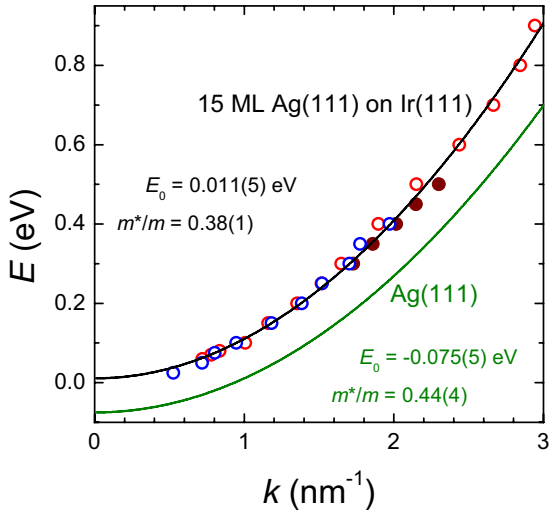

FIG. 2. (Color online) Dispersion relation of the silver surface state obtained on three different terraces on 15 ML Ag(111)/Ir(111). Dots stand for experimental STS maps. The black line represents a parabolic band with the two fitting parameters given in the figure (black). The olive (gray) colored dispersion is the band for Ag(111) as given by the olive (gray) colored parameters [28]. The filled dots correspond to the maps of Fig. 1.

shows a sharp kink around the Fermi energy. We attribute this prominent raise to the LDOS of the silver surface state [30], which has a steplike DOS characteristic for a parabolic band in 2D. The evaluation of the kink yields $E_0 \approx 0.05$ eV in agreement with the surface state energy at $k = 0$ obtained by mapping the energy-resolved Friedel oscillations on 15 ML Ag(111)/Ir(111) (see Fig. 2). The red (gray) spectrum recorded on gr/15 ML Ag(111)/Ir(111) shows a shifted kink that we attribute to the silver surface state surviving under graphene [14,31]. The kink is recorded at approximately 0.25 eV, meaning that the whole band shifts 0.2 eV towards higher energies. The evolution of the surface state when penetrating graphene can be seen best when recording a set of dI/dV spectra along a line beginning on the silver surface and ending on graphene [see the arrow in Fig. 3(a)]. The corresponding spectra are shown in Fig. 3(c). The spectra are stacked so that one can easily follow the behavior of the surface state when approaching and entering the graphene region. Beginning at the bottom of Fig. 3(c), the kink of the surface state is clearly visible near the Fermi energy (black spectra). Arriving at the border between silver and graphene, this signal first continuously vanishes, then reappears but shifted towards higher energies (red spectra).

In the following paragraphs, we will propose explanations for the two shifts of the silver surface state that we observe, namely, between 15 ML Ag(111)/Ir(111) and gr/15 ML Ag(111)/Ir(111) and between 15 ML Ag(111)/Ir(111) and Ag(111), starting with the latter. We propose that this shift is caused by epitaxial strain. Typically, such deformations of the crystal lattice are very difficult to detect using STM where lateral distances can only be obtained within an error of a few %. In our system, however, we can exploit the magnifying effect of the moiré superstructure [1,32] to determine the silver lattice constant. We find a strain of 1.0(6)% in the silver periodicity by evaluating the moiré pattern of a large, atomically resolved graphene island [33].

The strain in the silver layer can be linked to the shift of the surface state as shown in studies of an ultrathin silver layer on the Si(111)-(7 × 7) surface [34] and Ag(111) islands on Nb(110) [35]. They both report a similar shift of the surface state band and attribute it to a net strain in the silver lattice. The strain lifts the bulk band located at lower energies than the surface state, changing the whole projected bulk band gap. This influences the surface state since it has to stay in this gap, preserving the potential that confines it to the surface plane [34]. We propose that this mechanism is active for 15 ML Ag(111)/Ir(111). According to the model of Ref. [34], the strain which is necessary to shift the band to $E_0 = 0.01$ eV

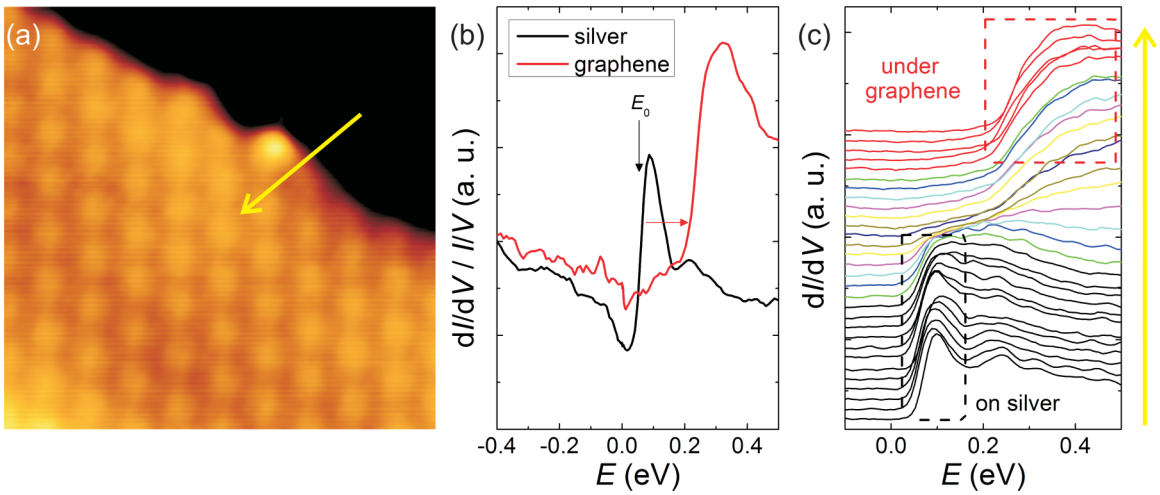

FIG. 3. (Color online) (a) STM image of the probed region of silver and graphene ($I = 0.4$ nA, $V = 0.2$ V, image size 14 × 14 nm^2). The arrow indicates the path of the tip to obtain the spectra. (b) Two normalized spectra (numbers 4 and 27 from the set) reveal the shift of the surface state when located under graphene ($I_{stab} = 0.081$ nA, $V_{stab} = 0.5$ V). The black arrow denotes the energy used to extract E_0 on the silver surface, while the red (gray) arrow illustrates the shift of the surface state under graphene. (c) 30 STS spectra, performed along the arrow in (a), from silver (bottom) to graphene (top). The dashed rectangles enclose the signal attributed to the Ag surface state.

is about 0.5%, in good agreement with the strain we measure with STM.

The second shift of of the silver surface state that we observe, namely, between 15 ML Ag(111)/Ir(111) and gr/15 ML Ag(111)/Ir(111), is comparable with the perturbation of the Ir(111) surface state under graphene [14,31], presumably due to the equivalent change of the boundary conditions for both surface states (from vacuum to a graphene boundary). We compare the influence of graphene with a chemically inert xenon layer on Ag(111) which results in a surface state energy shift of ≈0.12 eV towards higher energies [36]. Since xenon has a large band gap at the Fermi energy, no Coulomb potential effects induced by charge transfer can cause the shift there. However, these additional effects may cause the larger shift for graphene on Ag(111) where charge redistribution is present.

IV. CONFINEMENT ON GRAPHENE QUANTUM DOTS

In this section, we describe new effects that arise in the LDOS when graphene is present in the form of nanosized GQDs (see Fig. 4). In the topographic image [Fig. 4(b)], two GQDs (labeled A and B) have reached the surface of the silver film during heating but are still embedded in 1 ML of Ag. Point spectra taken on and next to the GQDs labeled A are shown in Fig. 4(b). The spectra on 15 ML Ag(111)/Ir(111) shows the characteristics of the Ag(111) surface state, whereas for gr/15 ML Ag(111)/Ir(111) the shoulder is shifted to higher energies (see arrows) and there is a substructure in the spectrum after the step: We observe a dip at 0.24 eV and new peaks around 0.315 and 0.50 eV. Mapping the LDOS at these particular energies reveals characteristic patterns, both on GQD A and B [see Figs. 4(c)–4(e)]. The energies of the maps are marked in the spectrum with blue (dark gray) lines. The interference pattern recorded on the embedding 15 ML Ag(111)/Ir(111) arise again from energy-resolved Friedel oscillations evolving at the step edges around the GQDs and around various defects.

We interpret the patterns observed in the spectroscopic maps as standing wave modes of states confined to the GQDs. In order to extract the underlying dispersion relation $E(k)$ from the observation of differently shaped eigenmodes at specific energies, we employ the following model: The confining potential is approximated as an infinite cylindrical well with radius $r = \sqrt{A/\pi}$ [see, e.g., the white dashed circle in Fig. 4(b)]. The confined wave functions Ψ that lead to the standing wave patterns $|\Psi|^2$ in the LDOS are assumed to be given by $\Psi_{m,l} \propto J_l(k_{m,l}\rho)e^{\pm il\phi}$ [in polar coordinates (ρ,ϕ)], where J_l is the spherical Bessel function of the first kind with order l [21]. Since the wave function has to vanish at the border of the GQD due to the infinite potential barrier, $\Psi_{m,l}$ must have a node for $\rho = r$, leading to the condition $k_{m,l}r = z_{m,l}$ with $z_{m,l}$ the mth zero of J_l, and so the eigenstates are labeled (m,l). The momentum $k_{m,l}$ of a given state (m,l) observed at an energy E can be calculated via $k_{m,l} = z_{m,l}/r = z_{m,l}\sqrt{\pi/A}$. All states with a certain (m,l) have a characteristic shape: (1,0) looks like a bubble, (1,1) like a ring, and (2,0) like a sombrero, to name a few. Following this model, the states of GQD A in Figs. 4(c) and 4(d) are (1,1) at 0.24 eV and (2,0) at 0.315 eV. The states of GQD B are (1,0) at 0.24 eV, (2,0) at 0.315 eV, and (3,0) at 0.5 eV.

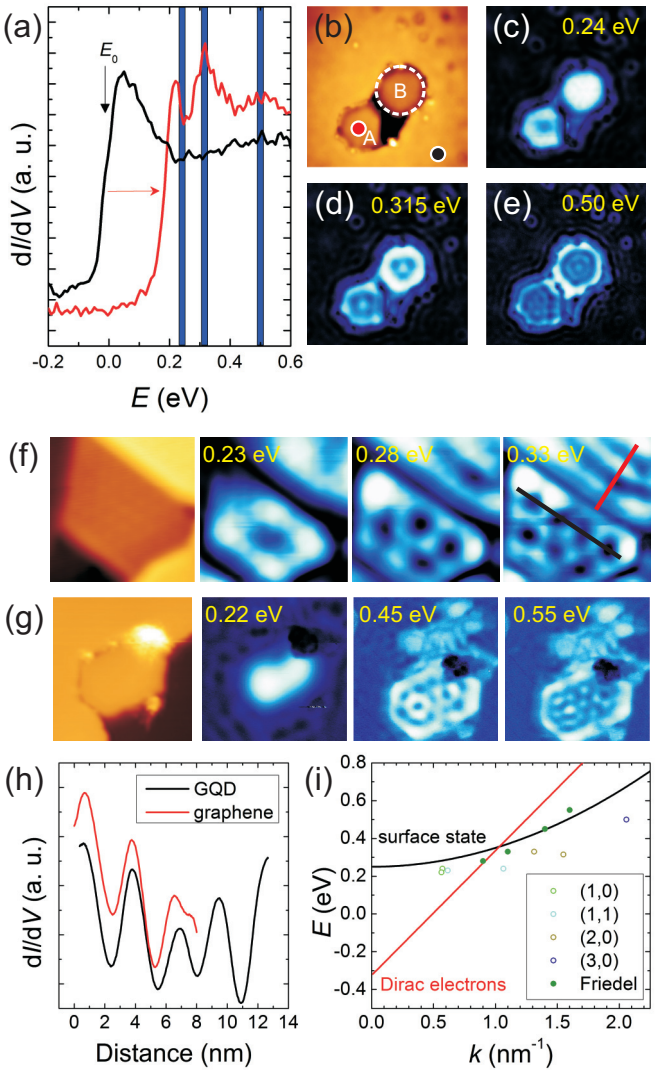

FIG. 4. (Color online) (a) dI/dV spectra recorded on silver (black) and on an embedded GQD ($I_{stab} = 0.1$ nA, $V_{stab} = 0.8$ V). The kink and shift of the surface state are visualized by two arrows. The three blue (dark gray) lines denote the energies which are mapped. Their width corresponds to ΔE. (b) STM image of two GQDs labeled A and B with two (small) circles indicating the probing places of the spectra and one (big) dashed circle illustrating the approximation of the Bessel model ($I = 0.1$ nA, $V = 0.5$ V, image size 28×28 nm^2). (c) STS map recorded at 0.24 eV revealing a confined ringlike (1,1) state on GQD A together with a bubblelike (1,0) state on GQD B. (d) The map recording the LDOS at 0.315 eV measures a (2,0) state on both GQDs, respectively. (e) A (3,0) state is recorded on GQD B at 0.50 eV. (f) Graphene confined by step edges ($I = 0.5$ nA, $V = 0.2$ V, image size 15×15 nm^2). Confined standing wave patterns are observed on the small terrace, while energy-resolved Friedel oscillations are recorded on the upper, larger terrace. (g) Standing waves recorded on a GQD at a step edge, which are unaffected by the adsorbates on the GQD ($I = 0.2$ nA, $V = 1$ V, image size 20×20 nm^2). (h) Comparison of the LDOS modulations of the two lines drawn in (f). (i) Dispersion relation extracted from the confined states and energy-resolved Friedel oscillations obtained on GQDs, together with the expected bands for the surface state and Dirac electrons.

A plot of $E(k)$ using the values determined according to the procedure explained above [Fig. 4(i), open symbols] reveals the underlying dispersion relation. We compare the experimental data with the bands present on GQDs: The red (gray) line in Fig. 4(i) represents the linear Dirac cone with $v_F = 10^6$ m/s and a Dirac point energy of $E_D = -0.325$ eV as found for gr/Ag(111) using density functional theory (DFT) [37]. The black line is the parabolic band of the silver surface state using $E_0 = 0.25$ eV as determined from point spectroscopy in Fig. 3(b) and $m^*/m = 0.38$ as determined from the analysis of the Friedel oscillations shown in Fig. 2. The much better agreement with the latter band is obvious. We conclude that the confined states arise from the surface state of silver under the GQDs and not from graphene itself, which can be explained with the high $k_\parallel$ of the Dirac electrons located near the K point which damps their contribution to the tunneling current [38]. This is the opposite behavior as found for GQDs in the system gr/O/Ir(111) where the confined states could clearly be attributed to the Dirac states of graphene [17]. A strong indication that the patterns are not due to Dirac states is that we do not observe them below the band of the surface state.

For eigenstates with high quantum numbers (m,l) and/or states on more irregular islands, the patterns in the LDOS become increasingly complex [see Figs. 4(f) and 4(g)]. An analysis based on the Bessel model is no longer possible in these cases. However, the patterns become more and more similar to the energy-resolved Friedel oscillations discussed in the previous section. This is shown in Fig. 4(f). The topographic image shows a part of an extended graphene flake covering a large (top right) and a small substrate terrace (center). States are confined by the substrate step edges. A ring is recorded at low energies. It is characterized as a (1,1) state within the Bessel model. With increasing E, the standing wave pattern becomes more complex, making it possible to directly read out the wavelength of the state. We use the Bessel model to compute k at small energies, while the corresponding wavelength is used at high energies in analogy to the energy-resolved Friedel oscillations. The equality of both models is visible in Fig. 4(h) which compares the wavelengths of the standing wave patterns recorded along the lines in Fig. 4(f): one is from a confined state, the other from energy-resolved Friedel oscillations recorded on the extended terrace partly visible in the STM image. This is a further indication that Dirac states do not play a role here, as the Friedel oscillations were unambiguously attributed to the surface state in our analysis above (see Fig. 2). Finally, the confined states are not disturbed by adsorbates located on GQDs as can be observed in Fig. 4(g). Although defects are present in the maps (as a featureless cloud), the standing wave pattern on the GQD seems to be unaffected by them. A similar finding was found for the surface state of iridium under graphene, which even persists in air due to the protective layer of graphene on top of it [31].

After we have established that GQDs can indeed confine the surface state of the metal substrate underneath, we speculate about the mechanism allowing this confinement. For the closely related phenomenon of a confined surface state in gr/Ir(111), it has been proposed in Ref. [14] that (i) the local gating of the surface state and (ii) the fact that carbon atoms at the edge of the GQDs are covalently bound to the substrate atoms [39] lead to quantum confinement. However, the latter seams unlikely for the case of gr/Ag(111) as corresponding DFT calculations [40] reveal that the interaction between the carbon edge atoms with the substrate is considerably weaker. In addition, for the chemically rather similar substrate Au(111), even a manipulation of GQDs with the STM tip is possible [16], further indicating a weak interaction. We conclude that the gating only is sufficient to confine the surface state, similar to the confinement of image potential states *above* GQDs on Ir(111) [41].

V. PARTIALLY SILVER INTERCALATED GRAPHENE QUANTUM DOTS

We now reduce the amount of intercalated silver by heating the sample for a short time above the desorption temperature of silver [42]. Figures 5(a) and 5(b) show two STM images obtained after heating at $T = 935$ K for 3 min and $T = 1125$ K

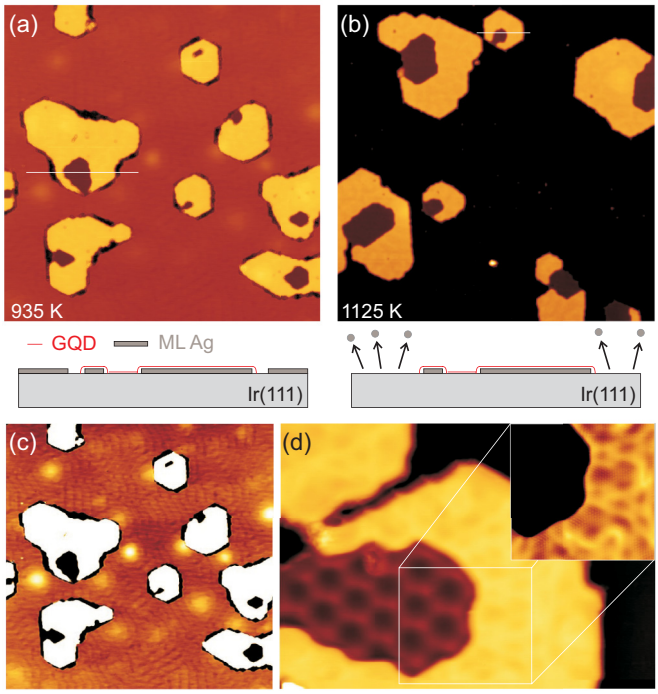

FIG. 5. (Color online) (a) STM image after heating to $T = 935$ K ($I = 0.1$ nA, $V = 0.92$ V, image size 111×111 nm^2). Partially silver intercalated GQDs are visible. A sketch under the STM image illustrates the side view of the morphology along a cut (horizontal line). (b) STM image of the same size recorded at a different place on the sample after an additional heating step at $T = 1125$ K ($I = 0.038$ nA, $V = 0.4$ V, image size 111×111 nm^2). Silver has desorbed next to GQDs, as shown in the side view. (c) Same image as in (a) with a different contrast to enhance the visibility of the silver reconstruction on Ir(111). (d) STM image showing a periodic moiré on gr/Ir(111) ($I = 0.05$ nA, $V = 0.4$ V, image size 28×20 nm^2). The magnification in the inset reveals an aperiodic corrugation on gr/1 ML Ag(111)/Ir(111) ($I = 0.09$ nA, $V = 0.4$ V, image size 12×11 nm^2). The color scale is the same in all STM images except (c): silver is red (light gray), intercalated graphene is yellow (very light gray), graphene on Ir(111) brown (dark gray), and Ir(111) black.

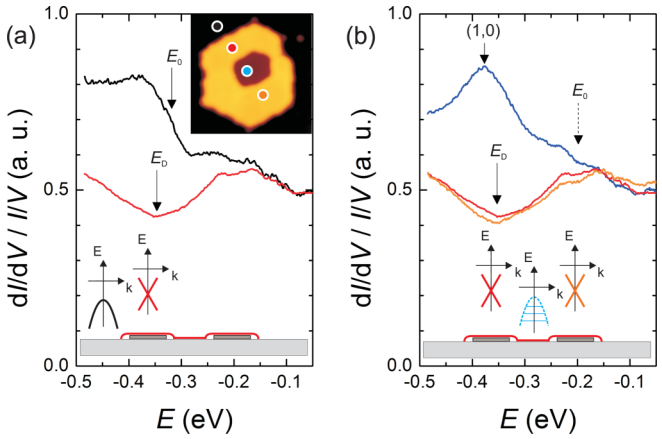

FIG. 6. (Color online) (a) Two spectra ($I_{stab} = 0.03$ nA, $V_{stab} = 0.125$ V) recorded on the places indicated by colored circles on the STM image in the inset ($I = 0.03$ nA, $V = 0.4$ V, image size 17.5×17.5 nm^2). The spectrum transforms from the black one showing a surface state kink (corresponding to E_0) to the red (light gray) one showing a Dirac dip (with a minimum at E_D). The sketch at the bottom shows the band responsible for the dominant contribution. (b) Three spectra probed on intercalated and nonintercalated graphene [marked in the inset of (a)] with the orange (very light gray) and the red (light gray) one [same as in (a)] showing a Dirac feature and the blue (dark gray) one showing a peak, respectively. The shifted E_0 of the Ir(111) surface state under extended graphene is highlighted with a dashed arrow.

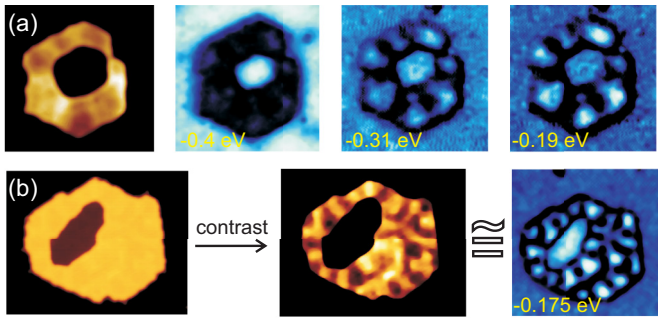

FIG. 7. (Color online) Corrugation dependence of the LDOS located on intercalated GQDs: (a) The STM (left, same as in Fig. 6) and STS images exhibit the same, energy-independent pattern on the intercalated phase ($I = 0.03$ nA, $V = 0.4$ V, image size 18×18 nm^2). A confined (1,0) state is visible at -0.4 eV on the nonintercalated phase. (b) A larger GQD showing the same effect ($I = 0.6$ nA, $V = 0.2$ V, image size 34×27 nm^2).

for a few seconds, respectively. Note that Ag and Ir do not form alloys due to the very small solubility of Ag in Ir (the most dilute alloys contain 1.8 at.% Ag) [43]. One ML of silver is still present after the first heating step due to the higher desorption temperature of the first ML of silver on Ir(111) [44]. The system 1 ML Ag(111)/Ir(111) shows a complex surface reconstruction as can bee seen in Fig. 5(c). In principle, such a reconstruction has a well-defined superstructure, albeit with a rather large unit cell, as observed in the similar system Ag/Pt(111) [45]. However, the presence of multiple rotational domains as well as the strong dependance on local strain can lead to patterns with no observable short-range periodicity in the corrugation. This is the case for 1 ML Ag(111)/Ir(111) [see Fig. 5(c)]. We observe that GQDs exhibit two phases and are surrounded by a gap. STS measurements performed on the lower (darker) graphene phase reveal the presence of the Shockley surface state of Ir(111) [as will be discussed in the context of Fig. 6(b)] which is absent on the higher (brighter) areas. We conclude that the higher phase is silver intercalated, while the lower phase represents graphene on Ir(111). The STM image shown in Fig. 5(d) confirms these findings, revealing a moiré pattern on gr/Ir(111) while an aperiodic structure is found on gr/1 ML Ag(111)/Ir(111) that we link to the surface reconstruction of 1 ML Ag(111)/Ir(111). The sketch under Fig. 5(a) visualizes the topography. Additional annealing at $T = 1125$ K leads to the desorption of silver next to graphene while the ratio of the two phases is nearly maintained. This is illustrated in the sketch under Fig. 5(b). Now, silver is present under GQDs only, and there only partially. In consequence, three different regions are present on the sample that we refer to as Ir(111), gr/Ir(111), and gr/1 ML Ag(111)/Ir(111).

To probe the LDOS of the surface, normalized dI/dV spectra are recorded at the places marked by dots in the inset of Fig. 6(a). The black spectrum in Fig. 6(a) obtained on Ir(111) shows a characteristic shoulder corresponding to the holelike surface state S_0 [14]. The extracted $E_0 \approx -0.33$ eV is in good agreement with the value of $E_0 \approx -0.34$ eV measured with ARPES [31]. The red (gray) spectrum obtained on a GQD formed by gr/1 ML Ag(111)/Ir(111) does not show any shoulder corresponding to a surface state, in contrast to the findings above for a thicker silver layer. Instead, a pronounced dip is found in the LDOS which we attribute to the vanishing DOS of graphene. The sketch in Fig. 6(a) illustrates the bands responsible for the features in the LDOS: While the holelike surface state dominates the LDOS next to the GQD, a clear contribution of Dirac electrons can be recorded on graphene.

We suggest that the suppression of the surface state originates from the aperiodic pattern due to the surface reconstruction observed on silver intercalated graphene [see Figs. 5(d) and 7]. This leads to aperiodic variations of the potential energy landscape, and in consequence to a strong suppression of the surface state as reported in Refs. [46,47].

Figure 6(b) compares spectra measured on gr/1 ML Ag(111)/Ir(111) with a spectrum obtained on gr/Ir(111). Both intercalated regions show the same Dirac feature, while a prominent maximum appears instead of a surface kink in the region where silver is absent. We propose that the peak represents the confined (1,0) state of the surface state of Ir(111) and verify our assumption by mapping the LDOS at $E = -0.4$ eV as shown in Fig. 7(a). The bubblelike confined state is clearly visible for gr/Ir(111). The confinement is illustrated in the sketch in Fig. 6(b) where only states at the crossing points between the quadratic band and the quantized horizontal lines contribute to the spectrum. Note that only the first line representing the energy of the (1,0) state is captured in our spectrum as a peak and that the Dirac cone is neglected in the middle sketch due to the dominant contribution of the surface state.

A discretization of the states on the confining gr/1 ML Ag(111)/Ir(111) area could in principle also be expected due to the small size of the intercalated flake. This would lead to peaks in the LDOS instead of a continuous dip as found in our spectrum. However, the potential energy landscape is very different to the case of gr/15 ML Ag(111)/Ir(111): There, two regions (with and without graphene on top) are clearly separated, leading to a well-defined potential well. In the case of gr/1 ML Ag(111)/Ir(111), we have (i) two regions on the GQD (with and without silver underneath), (ii) a local hybridization with the Ir(111) substrate at the rim of the GQD (leading to a soft confinement potential [15] rather than a hard wall), (iii) a region of interest with a very irregular shape (distorted ring), and (iv) an additional modulation due to the silver reconstruction. The contribution of the latter can be seen best in Fig. 7 displaying additional STS maps which record the LDOS on gr/1 ML Ag(111)/Ir(111): They always show a pattern strongly correlated to the corrugation of the GQD caused by the reconstructed surface underneath. The pattern is independent of energy, excluding a spatial mapping of the Dirac energy [48,49] where the pattern exhibits a contrast inversion when passing E_D. A similar corrugation-dependent pattern has been found for the moiré corrugation of gr/Ir(111) [15]. We propose that this ill-defined potential landscape smears out the sharp peaks expected for a state confined in an infinite potential well with well-defined geometry, leading to the observed spectrum, and explains the small variations found in the extracted Dirac energy between $E_D = -0.34$ and -0.37 eV.

VI. CONCLUSIONS

We have investigated the main contribution to the LDOS of gr/Ir(111), gr/1 ML Ag(111)/Ir(111), and gr/15 ML Ag(111)/Ir(111), and found that the metal surface state dominates the LDOS if present, masking the contribution of graphene.

The surface of 15 ML Ag(111)/Ir(111) exhibits a surface state with a dispersion relation comparable to the band of the Ag(111) Shockley surface state, but shifted up in energy (i) due to a net strain and (ii) when located under graphene. We have shown that it is possible to confine the surface state on GQDs by comparing the dispersion of the observed standing wave patterns with the quadratic band of the surface state and ruling out a contribution of the Dirac electrons of graphene.

A prominent Dirac feature is found on gr/1 ML Ag(111)/Ir(111) where the surface states of silver and iridium are suppressed, while a signal attributed to a holelike surface state is detected on Ir(111) and gr/Ir(111). The partially intercalated GQDs show an aperiodic corrugation. We interpret this as the cause of the energy-independent patterns that we observe by mapping the LDOS on these GQDs.

ACKNOWLEDGMENTS

This work was supported by the Deutsche Forschungsgemeinschaft through the Grants No. INST2156/514, No. BU 2197/2, and BU Grant No. 2197/4 inside SPP 1459 "Graphene." We acknowledge extensive support by T. Michely.

[1] J. Coraux, A. T. N'Diaye, C. Busse, and T. Michely, Nano Lett. **8**, 565 (2008).
[2] P. W. Sutter, J.-I. Flege, and E. A. Sutter, Nat. Mater. **7**, 406 (2008).
[3] L. Gao, J. R. Guest, and N. P. Guisinger, Nano Lett. **10**, 3512 (2010).
[4] M. Corso, W. Auwärter, M. Muntwiler, A. Tamai, T. Greber, and J. Osterwalder, Science **303**, 217 (2004).
[5] S. Helveg, J. V. Lauritsen, E. Lægsgaard, I. Stensgaard, J. K. Nørskov, B. S. Clausen, H. Topsøe, and F. Besenbacher, Phys. Rev. Lett. **84**, 951 (2000).
[6] H. G. Füchtbauer, A. K. Tuxen, P. G. Moses, H. Topsøe, F. Besenbacher, and J. V. Lauritsen, Phys. Chem. Chem. Phys. **15**, 15971 (2013).
[7] P. Vogt, P. De Padova, C. Quaresima, J. Avila, E. Frantzeskakis, M. C. Asensio, A. Resta, B. Ealet, and G. Le Lay, Phys. Rev. Lett. **108**, 155501 (2012).
[8] A. Varykhalov, J. Sánchez-Barriga, A. M. Shikin, C. Biswas, E. Vescovo, A. Rybkin, D. Marchenko, and O. Rader, Phys. Rev. Lett. **101**, 157601 (2008).
[9] I. Pletikosić, M. Kralj, P. Pervan, R. Brako, J. Coraux, A. T. N'Diaye, C. Busse, and T. Michely, Phys. Rev. Lett. **102**, 056808 (2009).
[10] Y. Zhang, T.-R. Chang, B. Zhou, Y.-T. Cui, H. Yan, Z. Liu, F. Schmitt, J. Lee, R. Moore, Y. Chen, H. Lin, H.-T. Jeng, S.-K. Mo, Z. Hussain, A. Bansil, and Z.-X. Shen, Nat. Nanotechnol. **9**, 111 (2014).
[11] B. Kiraly, E. V. Iski, A. J. Mannix, B. L. Fisher, M. C. Hersam, and N. P. Guisinger, Nat. Commun. **4**, 2804 (2013).
[12] S.-H. Phark, J. Borme, A. L. Vanegas, M. Corbetta, D. Sander, and J. Kirschner, ACS Nano **5**, 8162 (2011).
[13] S. K. Hämäläinen, Z. Sun, M. P. Boneschanscher, A. Uppstu, M. Ijäs, A. Harju, D. Vanmaekelbergh, and P. Liljeroth, Phys. Rev. Lett. **107**, 236803 (2011).
[14] S. J. Altenburg, J. Kröger, T. O. Wehling, B. Sachs, A. I. Lichtenstein, and R. Berndt, Phys. Rev. Lett. **108**, 206805 (2012).
[15] D. Subramaniam, F. Libisch, Y. Li, C. Pauly, V. Geringer, R. Reiter, T. Mashoff, M. Liebmann, J. Burgdörfer, C. Busse, T. Michely, R. Mazzarello, M. Pratzer, and M. Morgenstern, Phys. Rev. Lett. **108**, 046801 (2012).
[16] P. Leicht, L. Zielke, S. Bouvron, R. Moroni, E. Voloshina, L. Hammerschmidt, Y. S. Dedkov, and M. Fonin, ACS Nano **8**, 3735 (2014).
[17] W. Jolie, F. Craes, M. Petrović, N. Atodiresei, V. Caciuc, S. Blügel, M. Kralj, T. Michely, and C. Busse, Phys. Rev. B **89**, 155435 (2014).
[18] M. Papagno, P. Moras, P. M. Sheverdyaeva, J. Doppler, A. Garhofer, F. Mittendorfer, J. Redinger, and C. Carbone, Phys. Rev. B **88**, 235430 (2013).
[19] A. M. Shikin, V. K. Adamchuk, and K.-H. Rieder, Phys. Solid State **51**, 2390 (2009).
[20] G. M. Rutter, J. N. Crain, N. P. Guisinger, T. Li, P. N. First, and J. A. Stroscio, Science **317**, 219 (2007).

[21] M. F. Crommie, C. P. Lutz, and D. M. Eigler, Science **262**, 218 (1993).
[22] J. Coraux, A. T. N'Diaye, M. Engler, C. Busse, D. Wall, N. Buckanie, F.-J. Meyer zu Heringdorf, R. van Gastel, B. Poelsema, and T. Michely, New J. Phys. **11**, 039801 (2009).
[23] R. Feenstra, J. A. Stroscio, and A. Fein, Surf. Sci. **181**, 295 (1987).
[24] M. Morgenstern, Surf. Rev. Lett. **10**, 933 (2003).
[25] M. F. Crommie, C. P. Lutz, and D. M. Eigler, Nature (London) **363**, 524 (1993).
[26] Y. Hasegawa and P. Avouris, Phys. Rev. Lett. **71**, 1071 (1993).
[27] P. T. Sprunger, L. Petersen, E. W. Plummer, E. Lægsgaard, and F. Besenbacher, Science **275**, 1764 (1997).
[28] R. Paniago, R. Matzdorf, G. Meister, and A. Goldmann, Surf. Sci. **336**, 113 (1995).
[29] L. Petersen, P. T. Sprunger, P. Hofmann, E. Lægsgaard, B. G. Briner, M. Doering, H.-P. Rust, A. M. Bradshaw, F. Besenbacher, and E. W. Plummer, Phys. Rev. B **57**, R6858 (1998).
[30] J. Li, W.-D. Schneider, and R. Berndt, Phys. Rev. B **56**, 7656 (1997).
[31] A. Varykhalov, D. Marchenko, M. R. Scholz, E. D. L. Rienks, T. K. Kim, G. Bihlmayer, J. Sánchez-Barriga, and O. Rader, Phys. Rev. Lett. **108**, 066804 (2012).
[32] A. T. N'Diaye, J. Coraux, T. N. Plasa, C. Busse, and T. Michely, New J. Phys. **10**, 043033 (2008).
[33] See Supplemental Material at http://link.aps.org/supplemental/10.1103/PhysRevB.91.115419 for a detailed analysis of the strain.
[34] G. Neuhold and K. Horn, Phys. Rev. Lett. **78**, 1327 (1997).
[35] T. Tomanic, C. Sürgers, R. Heid, M. Alcántara Ortigoza, K.-P. Bohnen, D. Stöffler, and H. v. Löhneysen, Appl. Phys. Lett. **101**, 063111 (2012).
[36] H. Hövel, B. Grimm, and B. Reihl, Surf. Sci. **477**, 43 (2001).
[37] G. Giovannetti, P. A. Khomyakov, G. Brocks, V. M. Karpan, J. van den Brink, and P. J. Kelly, Phys. Rev. Lett. **101**, 026803 (2008).
[38] T. O. Wehling, I. Grigorenko, A. I. Lichtenstein, and A. V. Balatsky, Phys. Rev. Lett. **101**, 216803 (2008).
[39] P. Lacovig, M. Pozzo, D. Alfè, P. Vilmercati, A. Baraldi, and S. Lizzit, Phys. Rev. Lett. **103**, 166101 (2009).
[40] Y. Li, W. Zhang, M. Morgenstern, and R. Mazzarello, Phys. Rev. Lett. **110**, 216804 (2013).
[41] F. Craes, S. Runte, J. Klinkhammer, M. Kralj, T. Michely, and C. Busse, Phys. Rev. Lett. **111**, 056804 (2013).
[42] N. R. Gall, E. V. Rut'kov, and A. Y. Tontegode, Int. J. Mod. Phys. B **11**, 1865 (1997).
[43] I. Karakaya and W. T. Thompson, in *Binary Alloy Phase Diagrams*, 2nd ed., edited by T. B. Massalski, H. Okamoto, P. R. Subramanian, and L. Kacprzak (ASM International, Materials Park, 1990), pp. 49–50.
[44] N. R. Gall', E. V. Rut'kov, and A. Y. Tontegode, Phys. Solid State **46**, 371 (2004).
[45] S. Gestermann, M. Nohlen, M. Schmidt, and K. Wandelt, Surf. Rev. Lett. **04**, 1179 (1997).
[46] E. Bertel and U. Bischler, Surf. Sci. **307–309**, 947 (1994).
[47] R. Fasel, P. Aebi, R. G. Agostino, L. Schapbach, and J. Osterwalder, Phys. Rev. B **54**, 5893 (1996).
[48] A. Deshpande, W. Bao, F. Miao, C. N. Lau, and B. J. LeRoy, Phys. Rev. B **79**, 205411 (2009).
[49] H. Zhang, Q. Fu, Y. Cui, D. Tan, and X. Bao, J. Phys. Chem. C **113**, 8296 (2009).